PREDICTING EXPLOSION-GENERATED *Sn* AND *Lg* CODA USING SYNTHETIC SEISMOGRAMS

Ileana M. Tibuleac[1], Anastasia Stroujkova[2], Jessie L. Bonner[2], Kevin Mayeda[2], and James Britton[2]

University of Nevada at Reno[1] and Weston Geophysical Corporation[2]

Sponsored by National Nuclear Security Administration
Office of Nonproliferation Research and Development
Office of Defense Nuclear Nonproliferation

Contract No. DE-AC52-05NA26610[1,2]

ABSTRACT

Recent examinations of the characteristics of coda-derived *Sn* and *Lg* spectra for yield estimation have shown that the spectral peak of Nevada Test Site (NTS) explosion spectra is depth-of-burial dependent, and that this peak is shifted to higher frequencies for Lop Nor explosions at the same depths. To confidently use coda-based yield formulas, we need to understand and predict coda spectral shape variations with depth, source media, velocity structure, topography, and geological heterogeneity. Thus, we have undertaken a coda modeling study to predict *Sn* and *Lg* coda.

During the initial stages of this research, we have acquired and parameterized deterministic 6º x 6º velocity and attenuation models for the Nevada, Shagan, Degelen, Novaya Zemlya, and Lop Nor Test Sites. Near-source data are used to constrain density and attenuation profiles for the upper five km at several test sites. The upper crust velocity profiles are quilted into a background velocity profile at depths greater than five km. Topography from digital elevation models will eventually be incorporated into the model development. The models are parameterized for use in a modified version of the Generalized Fourier Method in two and three dimensions (GFM2D/3D). The new GFM algorithm will soon include a coordinate transform that allows for variable gridding in the upper few kilometers of the model and simulation of the topography at finer scales. The smaller grid size in the upper crust allows for an increase in the accuracy of the *Sn* and *Lg* synthetics.

We modify these models to include stochastic heterogeneities of varying correlation lengths within the crust. Three parameters—correlation length, Hurst number, and fractional velocity perturbation of the heterogeneities—are used to construct different realizations of random media. Building the stochastic model is not trivial, since a large number of medium and source-specific parameters affect the results. We discuss possibilities for heterogeneity parameter estimation using available seismic and geological data. Lateral correlation and coherence measures between seismic traces are estimated from clusters of nuclear explosions and well-log data. This, and information from elevation and geological maps, as well as satellite imagery, are used to generate synthetic waveforms we compare to the observed data. We assess the relative importance of variables such as heterogeneity location, model grid size, stochastic model parameters, and source type and depth in shaping the *Lg* coda.

Multiple runs with different realizations of stochastic velocity are needed to calculate average amplitude envelopes of the seismic traces for every set of the stochastic parameters. We calibrate these parameters by matching synthetic earthquake *Sn* and *Lg* coda envelopes to local earthquakes with well-defined moments and mechanisms. Once the deterministic and stochastic models have been generated, we will use GFM2D/3D to generate regional-distance synthetics for monopole explosions at depths ranging from 0.25 km to 1 km for all test-site models. We will then superpose secondary source effects, such as spall and compensated linear-vector dipole (CLVD) sources, on the monopole synthetics. Finally, we will derive *Sn* and *Lg* coda spectra from the synthetics, estimate moments, and yields from these spectra, and compare to observed data from each test site. If successful, this method may be used to estimate the *Sn* and *Lg* coda properties for yield estimation of explosions at historical test sites or for broad, uncalibrated regions where we will likely have little information on velocity structure.

OBJECTIVE

Our objective is to determine why the current mechanisms for *Sn* and *Lg* generation from explosions often produce stable coda magnitudes that are transportable between test sites. We aim is to understand and predict *Lg* and *Sn* coda spectral shapes with variations in source depth, material properties, velocity structure, topography, and geological heterogeneity. We will use 2D/3D modeling techniques to estimate synthetic explosion coda for five nuclear test sites as well as for regions without nuclear testing history.

RESEARCH ACCOMPLISHED

For sparse local and regional seismic networks and small events (< ~1 kt), one of the most stable and unbiased methods for yield and magnitude estimation is based on *Sn* and *Lg* coda envelopes (Mayeda, 1993). Coda-derived spectra have characteristics that require in-depth investigation, so that any possible bias can be accounted for when lower bounds on yields are reported. For example, the peaks of coda-derived Nevada Test Site (NTS) and Lop Nor explosion spectra are depth-of-burial dependent, however, the peaks are shifted to higher frequencies at Lop Nor.

We plan to compare observed local and regional *Sn* and *Lg* coda spectra to coda-derived source spectra for simulated explosions at the Nevada (NTS), Shagan (STS), Degelen (DTS), Novaya Zemlya (NZ) and Lop Nor (LN) Test Sites. Our coda investigation methodology consists of: 1) Compilation and parameterization of seismic velocity models consisting of deterministic material models with stochastic perturbations. Estimation of the effect of deterministic and stochastic model parameters on *Lg* propagation and structure; 2) Calibration of stochastic variations at the each test site using nearby earthquake data. Synthetic waveforms are created using a Generalized Fourier Method (GFM; Orrey et al., 2002) and 3) Calculation of 2D/3D synthetics for composite source models of varying depths and moments for each test site. An illustration of our progress in developing this methodology is presented below with results for earthquakes that occurred at the Nevada Test Site.

Methodology for Nevada Test Site Earthquakes and Explosions

Data. *Lg* coda from an earthquake recorded at MNV that occurred on June 29, 1992, 10:31:02.4 is modeled using combined deterministic and stochastic velocity models for the NTS-MNV (Mina, Nevada) path. This m_b 4.3 magnitude earthquake was a 5 km deep aftershock of the M_L 5.6 – 5.8 Little Skull Mountain, Nevada, June 29,1992, earthquake, which occurred in the SW portion of NTS, 20 km from Yucca Mountain. The aftershock was located 256.8 km from MNV, at a back azimuth of 138.2 deg. We assume that the aftershock and the main event located near Little Skull Mountain have the same mechanism, which was listed in the Harvard Centroid Moment Tensor (CMT) catalog. We used these CMT parameters to generate synthetic seismograms for the aftershock. A second earthquake occurred on June 14, 2002, 12:40:44 and recorded at NV11 (a station of the Mina, Nevada seismic array NVAR located less than 100 m from MNV), is used for comparison of the *Lg* coda.

To evaluate stochastic model parameter estimation using correlation of well-located event sequences, we use a dataset provided by Lawrence Livermore National Laboratory (LLNL), (Springer et al., 2002) of 247 NTS nuclear explosions ranging from 200-1500 m depth, recorded at MNV. Seismic velocities derived from geophone logs in boreholes 0.8 km deep at Pahute Mesa are also used to estimate shallow stochastic parameters. This database (Fergusson et al., 1994) was provided by Los Alamos National Laboratory.

Models. *Lg* coda for the events near Little Skull Mountain is modeled using deterministic and combined deterministic and stochastic velocity models for the path between NTS and MNV.

Deterministic Model Generation. The background velocity structure for NTS (see Figure 1; Tibuleac et al., 2005) is based on a regional model for the Basin and Range similar to the model developed by Benz et al. (1991). The velocities in the upper crust are based on borehole data, geologic and gravity data, refraction studies and seismic experiments (McLaughlin et al. 1983; Stump and Johnson, 1984; Ferguson et al., 1994; Stevens et al., 1991). The model is parameterized for use in *GFM 2D*, with grid spacing of either 0.25 km or 0.125 km. The 0.250 km grid has 1183 nodes in the X direction (~298 km) and 385 nodes (~96 km) in the Z direction, for a total of 0.45 million nodes. For this grid spacing, we are able to accurately model *Lg* up to 1.6 Hz. The 0.125 km grid has a total of 1.5 million nodes and can accurately model *Lg* up to 3.2 Hz. The edges of the grid have absorbing boundary conditions

to suppress artificial reflections. To avoid edge effects, the actual side boundaries of the grid are located 40 grid points (for 0.250 km grid spacing) and 70 grid points (for 0.125 km grid spacing) from either end of the model.

Stochastic Model Generation. Generating stochastic models (Tibuleac et al., 2005) is not trivial, considering the number of variables involved. Given the time required to run a model (4 hrs. for 0.250 km grid, 36 hrs for 0.125 km grid, 2D) we simultaneously investigate a) using seismic information in the region, to constrain the stochastic model parameters; and b) efficiently modifying the model for a best fit of the observed envelopes. We will combine the results of these calculations to build the final stochastic model.

Using Existing Seismic Information in the Region to Constrain Stochastic Model Parameters. To address the non-uniqueness inherent in our method, stochastic parameters at each test site are restricted within the bounds of the results from literature searches and satellite imagery correlation-length analyses. Since this information is not always available, it is important to evaluate alternative methods for stochastic parameter development such as correlation and coherence studies and well-log data.

Crosscorrelation Studies. We have estimated model stochastic parameters by correlating well-located nuclear explosions on NTS. This technique will be further applied, with appropriate modifications, to earthquakes in regions with no history of nuclear testing. We use seismograms from three clusters of NTS nuclear explosions as a virtual seismic array that records seismograms from a single source located at the real seismic receiver (the seismic station MNV). Source and receiver positions are virtually interchangeable because of the reciprocity of the Green's function of elastodynamics. We assume differences in phase characteristics (such as *Pn, Pg* and *Lg*) to reflect scattering from stochastic heterogeneity beneath the 'virtual array'.

We assume that the phase crosscorrelation maxima variation as a function of inter-event distance reflects a von Karman (Pullammanapalil, 1997) distribution of seismic velocity heterogeneity in the media. The maximum value of the absolute crosscorrelation of normalized and filtered (0.6 – 1.5 Hz and 0.6 – 4 Hz) waveforms in equal length *Pn, Pg* and *Lg* windows of each two events is averaged as a function of event separation (offset). The crosscorrelation maxim for the normalized entire event waveforms is also calculated. We use explosions within the same depth range (0.1 – 0.2 km; 0.2 – 0.4 km; 0.4 – 0.6 km; 0.6 – 0.8 km and 0.8 – 1.5 km) to estimate horizontal correlation.

Maxim crosscorrelation variation averaged to yield a single value at each spatial lag as a function of horizontal inter-event distance is shown in Figure 2. Since we are interested in the mean properties of the region, the figure is a summary of the results for all three clusters and all depth intervals. The von Karman correlation length for *Lg* phases is between 0.4 -1.1 km, with Hurst numbers (Pullammanapalil, 1997) between 0.3 and 0.7 for waveforms in two frequency intervals. We obtain inconsistent *Pn* results, possibly because the maxim crosscorrelation value for the *Pn* arrivals is the maxim value of the source function crosscorrelation (see explanation below) and does not vary with distance. At 256 km from NTS, *Pn* is a very weak and short phase, which might affect the results. Also, the real medium could have more than one fractal dimension as well as more than one correlation length or could be described by a distribution that is not von Karman The *Pg* correlation function variation is not a good approximation of a von Karman variation. Our experiments with waveforms generated by convolving random Green's functions with a random source function show that saturation of the crosscorrelation maxim values in Figure 1 is partly due to source similarity.

Coherence Studies. For NTS nuclear explosions we also measure seismic phase coherence (*Pg, Lg direct, Lg coda*) in different frequency ranges and estimated dominant heterogeneity dimensions. Direct wave scattering on heterogeneity inside the Earth produces coda (Nishizawa et al., 1997) and the energy transfer is controlled by the scattering characteristics of the media. Coda is the most coherent for most efficient scattering, when the wavelength λ is proportional to the size of heterogeneity *d* (Yomogida et al., 1998), that is, for

$$\frac{\lambda}{\pi} < d < \frac{3\lambda}{2\pi}$$

Therefore, dominant heterogeneity scale can be determined from the coherence maxima. The exact relationship between dominant heterogeneity dimension and von Karman correlation length is still to be established; however,

some authors consider the dominant heterogeneity dimension as the correlation length. Maxim coherence frequency is estimated in two cases: 1) horizontal coherence.for nuclear explosions at the same depth in each region and 2) vertical coherence, for nuclear explosions with $m_b < 5$ at different depth in 2 km^2 regions on the surface. Heterogeneity dimension is estimated to be between 0.7 and 1.9 km for raw *Pg* and between 0.2 and 1.8 km for *Lg* arrivals on the horizontal and vertical direction for the same set of 247 nuclear explosions. Waveform coherence function in the same region varies for each phase. A consistent feature is the *Lg* coda coherence, which is best between 1 and 4 Hz.

Auxillary Data Studies: Borehole Velocity Analysis. We use seismic velocity derived from geophone logs in boreholes at Pahute Mesa to estimate vertical stochastic media parameters at NTS (see Fergusson et al., 1994 for the borehole location).Whether to remove the general trend in the borehole data is not generally agreed upon (Dollan et al., 1998). We have performed our calculations with and without the general velocity trend removed. We assume the horizontal velocity variations are small and randomly distributed with depth within the 15 km length borehole region. The mean of autocorrelation borehole velocity functions is shown in Figure 2 (blue line). Von Karman correlation functions with parameters shown in Table 1 are the best L1 fit (measurement of fit of model to data) to the observed data and are represented with red lines in both plots. The Hurst number is very similar in both cases, however, the correlation length is twice as large for the case when the general trend is not removed. Our results from well log data are consistent with strong shallow heterogeneity with short wavelengths and are well modeled by a von Karman distribution.

Table 1. Von Karman distribution parameters from L1 interpolation of the mean autocorrelation curves in Figure 1. The vertical correlation is a_z (km) and the Hurst number is H. These values are valid down to 800 m depth.

General trend removed		**General trend not removed, each mean removed instead**	
a_z(km)	**H**	**a_z (km)**	**H**
0.04	0.6	0.08	0.5

Efficiently Modifying the Model for a Best Fit of the Observed Envelopes. It is important to model the entire *Lg* phase for best fit of the synthetic and observed waveforms. Mayeda and Walter, (1996) use the *Lg* envelope starting with the *direct Lg* maxim amplitude up to tens to several hundreds of seconds into the coda for coda magnitude estimation. Also, results from numerous studies (Rautian and Khalturin, 1978; Sherbaum et al., 1991; Spudick and Botswick, 1987; Der et al., 1984; Dainty and Tocksoz, 1990; Xie, 1996 and Shapiro et al., 2002) suggest that the *Lg* phase is composed of the least of two regimes. The earliest part of the *Lg*, the *direct Lg*, is spatially more coherent and composed of forward scattered waves with the same direction as the *S* waves and coda, arriving from a variety of directions.The early portion of coda is different from station to station; however, the coda of band-pass filtered seismograms have a common shape at all stations after about two times and always after three times the S-wave travel time from the source to the receiver. The later part of the coda tends to be comprised of multiple scattered waves and is described as a diffusion regime.

Out of a large number of possibilities, we identify the deterministic and stochastic parameters most likely to shape *Lg* and *Lg* coda. We design experiments to evaluate the effect of heterogeneity distribution in the crust on the *Lg* envelope. Effects of source mechanism and depth on coda are further quantified. While our focus remains *Lg* coda modeling, when choosing the best heterogeneity distribution and parameters we aim for the synthetic waveforms to also fit the first arrivals and their coda.

The Effect of Heterogeneity Location on Lg coda. To determine the location of the stochastic perturbations which most influence *Lg* coda, we construct models with different perturbation location within the crust (Table 2). The first model, SD1 has perturbations located at the Conrad discontinuity (from 15 km to 21 km deep). SD2 contains perturbations on top of the Moho, between 29.8 km and 32 km depth. We use a correlation length of 0.8 km with 10% velocity variation for the SD2 model. SD3 has stochastic perturbations distributed throughout the entire crust. Receivers are 0.5 km deep for model SD4 laying on the top of 1-km thick stochastic perturbations. Before the variable grid is implemented into GFM, using model SD4 was the closest to simulate topography effects. Model SD5 has perturbations confined to the upper 6 km of the crust. All the models, except for SD4, have receivers at the surface. We choose fractional perturbation of 10% for both velocity and density. Intrinsic attenuation was not added to these models. Our parameter choice is in accord with the stochastic parameters derived for the observed data.

Table 2. Stochastic parameters for the models used for synthetic waveform generation. We choose the notation SD to represent a stochastic model superposed on the deterministic model described by Tibuleac et al. (2005). D is depth (km), a_x is horizontal correlation length, a_z is vertical correlation length, % represents the fractional velocity and density perturbation in each model and H is the Hurst number. The stochastic layers in the models are represented by "x."

Depth km	Parameters				Models				
	$a_{x\ (km)}$	$a_{z\ (km)}$	H	%	SD1	SD2	SD3	SD4	SD5
0-0.5	0.5	0.25	0.5	10	-	-	x	-	x
0.5-1.5	0.5	0.25	0.5	10	-	-	x	x	x
0-1.5 - 3	0.5	0.25	0.5	10	-	-	x	-	x
3-4	0.6	0.3	0.5	10	-	-	x	-	x
4-5.5	0.6	0.3	0.5	10	-	-	x	-	x
5.5-6	0.8	0.3	0.5	10	-	-	x	-	x
6-15	0.8	0.3	0.5	10	-	-	x	-	-
15-21	1	0.3	0.5	10	x	-	x	-	-
6-24.4	1	0.3	0.5	10	-	-	x	-	-
24.4-27.8	0.8	0.8	0.5	10	-	-	x	-	-
27.8-29.8	0.8	0.8	0.5	10	-	-	x	-	-
29.8-32	1	0.3	0.5	10	-	x	-	-	-
32+	-	-	-	-	-	-	-	-	-

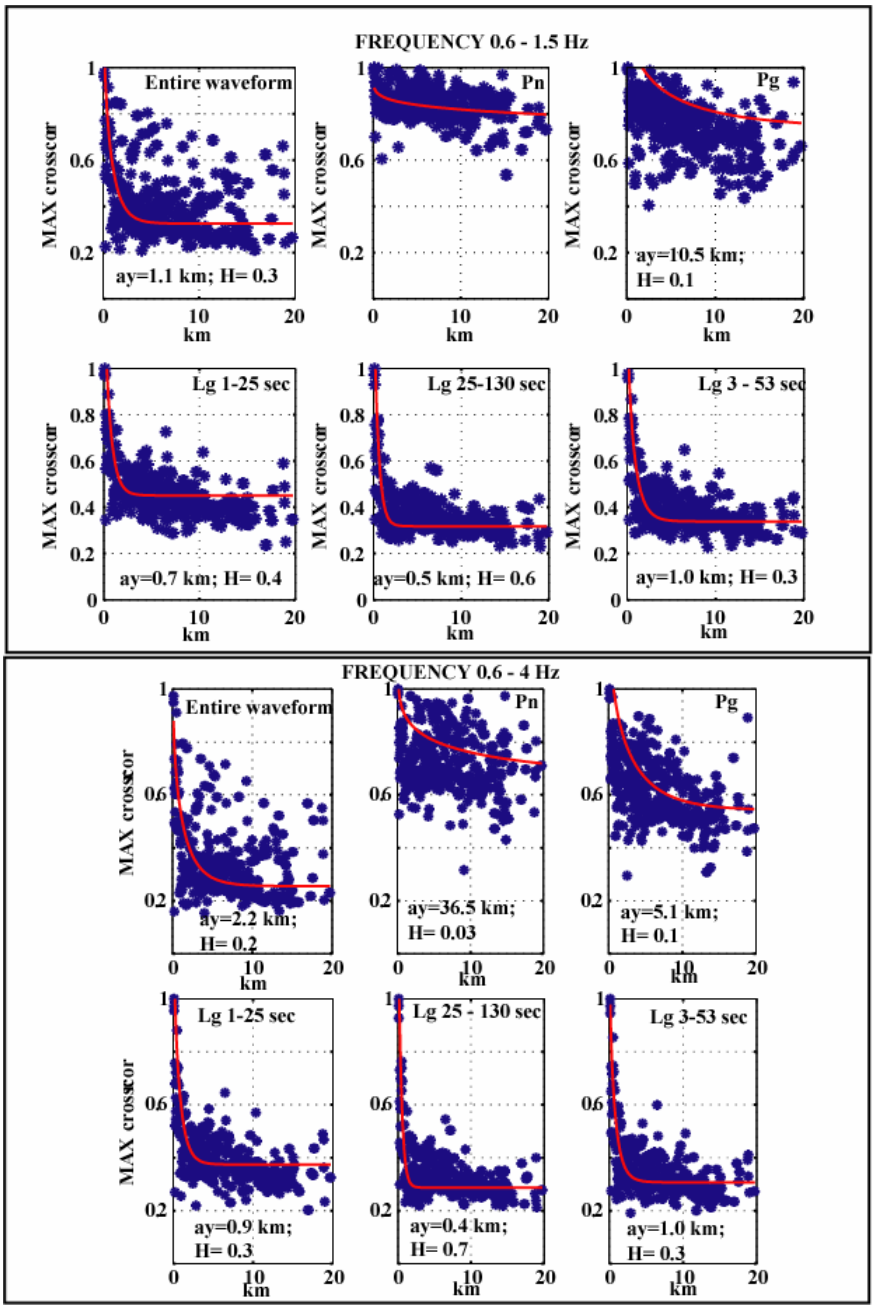

Figure 1. Variation of the crosscorrelation maxima with inter-event distance in a frequency range of 0.6 – 1.5 Hz (upper plots) and 0.6 – 4 Hz (lower plots) for the whole waveform (upper left plot), *Pn* window (upper middle plot), *Pg* window (upper right plot), direct *Lg* window (lower left plot), *Lg* coda window (middle plot) and the transitional *Lg* arrival (right plot). The crosscorrelation maxima as a function of inter-event distance are calculated for each of the depth intervals and the results are shown here for all depths and all clusters. The continuous line represents the L1 interpolated von Karman model correlation variation with the saturation value added. The estimated horizontal correlation value (a_y) and the Hurst number (H) are represented in each plot. The unrealistic values estimated for the *Pn* are omitted. Note the offsets are much larger than the characteristic length, therefore we have a robust measure of the correlation function.

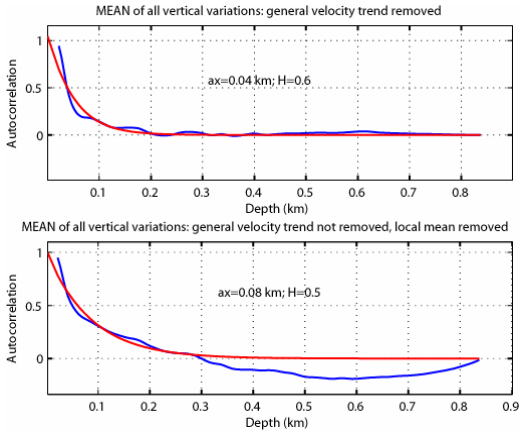

Figure 2. Upper plot: Autocorrelation mean for all wells (blue) and the L1 norm fit (red) of a von Karman autocorrelation function. The general velocity trend was removed at each well. Lower plot: Autocorrelation mean for all wells (blue) and the L1 norm fit (red) of a von Karman autocorrelation function when the general trend was not removed. The von Karman parameters of the best fit are shown in each plot.

Figure 3 shows a comparison of the observed waveforms (g and h) and the synthetic waveforms without (a) and with (b-f) random velocity variations in the model for 0.250 km grid. In the three upper plots, we observe large 1-Hz surface waves that are typically not observed in regional data near NTS. Adding crustal heterogeneity (d-f) forward- and back scatters more energy into the *Lg* coda. The best correspondence of synthetic and observed *Lg* coda is obtained for a model with stochastic heterogeneity only in the upper 6 km of the crust (f). Adding heterogeneity into the whole crust (d) produces more scattering than in the recorded waveform, mostly for first arrivals. Variable heterogeneity in a 1 km thick layer on top of the crust affects more the later part of *Lg* coda (however, the resulting coda amplitude is ten times less than the SD5 coda amplitude) and affects less the direct *Lg*.

Significant amplitude noise is observed before the event for models SD3 and SD5. The inaccuracy of the GFM method at high frequencies produces frequency-dependent errors in phase and group velocity, i.e. 'grid dispersion' (Frankel and Clayton, 1986). The errors are a function of the wavelength to grid spacing ratio and can produce effects in the synthetic seismograms similar to those of attenuation. We observe that a smaller grid size model reduces the amplitude of numerical noise. However, a comparison of waveforms propagated through the SD5 model with 0.25 km and 0.125 km grid spacing shows that the finer grid produces a lower amplitude event signal as well as slightly more coda. One possible reason is that the variance in a medium with a finer grid depends on the Nyquist wavenumber $k_{Nyq} = \pi / h$, where h is the grid spacing (Frankel and Clayton, 1986, eq. B2). The variance of a finer sampled medium is larger. In the spatial domain it is equivalent to truncating the correlation function at zero offset. Therefore, future investigations will address normalization of the discrete random media to correspond to a continuous media with a given variance.

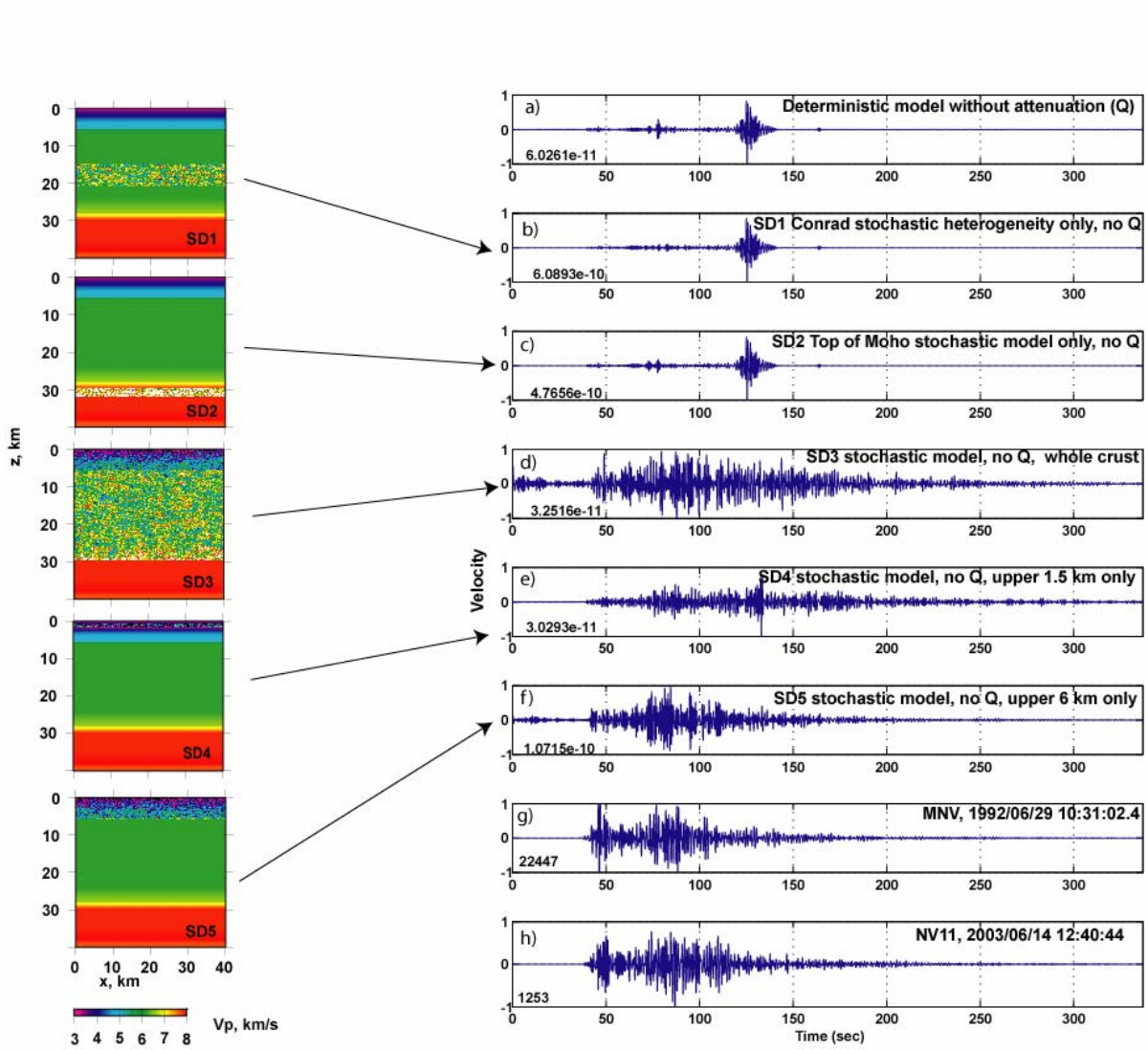

Figure 3. (Left) Stochastic models superposed on the deterministic model used for *Lg* coda simulations. (Right) A comparison of observed waveforms (g,h) and synthetics propagating in the 2D NTS-MNV velocity model without (a) and with (b-f) stochastic variations. The *Lg* phase arrives at a time lag of 73 sec. Waveforms represent velocity in nm/s filtered from 0.5 to 1.6 Hz with a zero-phase, 4 pole Butterworth forward and reverse filter. The waveforms are normalized to the largest *Lg* amplitude value (shown in the lower left corner) between 0.5 and 1.6 Hz. Large 1 Hz surface wave arrivals at 140 seconds lag (upper three plots) are removed by introducing stochastic perturbations in the deterministic model. In plots (d-f) more energy is scattered in the *Lg* coda. Note low-amplitude direct-wave *Lg* arrivals when the stochastic heterogeneity is located at the Conrad depth.

The Effect on Direct Lg of Moho Depth and Seismic Velocity Value at the Surface. If the direct *Lg* and coda waveforms propagate through the same parts of the crust, an SD5 model with 65 km deep crust will affect direct *Lg* as well as its coda. On the contrary, if coda is formed mostly at the surface, where 3 km/s velocities dominate, then a higher velocity (6 km/s) in the upper 6 km of model SD5 will mostly affect coda. Our simulations show that a high-velocity upper layer with stochastic composition (same parameters as for SD5, with 6 km/s in the upper layer instead of 3 km/s) significantly diminishes both *Pg* and *Lg* coda while a 65-km deep Moho does not significantly affect the *Lg* coda. Also, reverberations from Moho are present following direct *Lg*, however Moho depth is a less important factor in the coda envelope shape than the upper layer seismic velocity.

The Effect of Source Mechanism on Lg Coda. An explosion source mechanism is also used in model SD5 and the results are compared to the two recorded events at MNV and NV11 described in Figure 4. We observe that source mechanism has a slight effect on *Lg* coda envelope shape for double-couple and explosion-type sources at the same depth (Figure 4, first and sixth plots in upper inset). Source mechanism is important for event amplitude and the shape and amplitude of the first arrivals. Further investigations are necessary to quantify these effects.

The Effect of Source Depth on Coda. Earthquake and explosion sources were placed at different depths in the SD5 model, with 0.250 km and 0.125 km grid spacing. A decrease in coda high-frequency content with depth is observed for different explosions in the NTS velocity model. Figure 4 shows explosions at different depths in the SD5 model. Depth effects are better modeled using a finer grid (Figure 4, second inset, grid size 0.125 km).

Effects of Variable Correlation Lengths on Direct Lg and Lg Coda. Synthetic waveforms from models with correlation lengths two, four, and eight times larger than in the SD5 model with 0.250 km grid spacing (with the same aspect ration on vertical and horizontal) show that the longer the correlation length, the higher the relative energy in longer wavelengths and the longer the coda duration.

Effects of Variable Hurst Numbers on the Envelope and Frequency of Direct Lg and Lg Coda. Synthetic waveforms from models with characteristic Hurst numberS 0.3 and 0.8 are compared to waveforms from model SD5. The Hurst number is important for amplitude as well as for the shape of the coda. The more rugged the medium (lower H) the more high-frequency coda is observed**.**

Effects of Seismic Velocity Perturbations on Coda Frequency and Amplitude. We observe important effects of heterogeneity dimension on the coda. We observe lower amplitude, longer coda when the 10% velocity perturbation in model SD5 is replaced with 5% velocity perturbation.

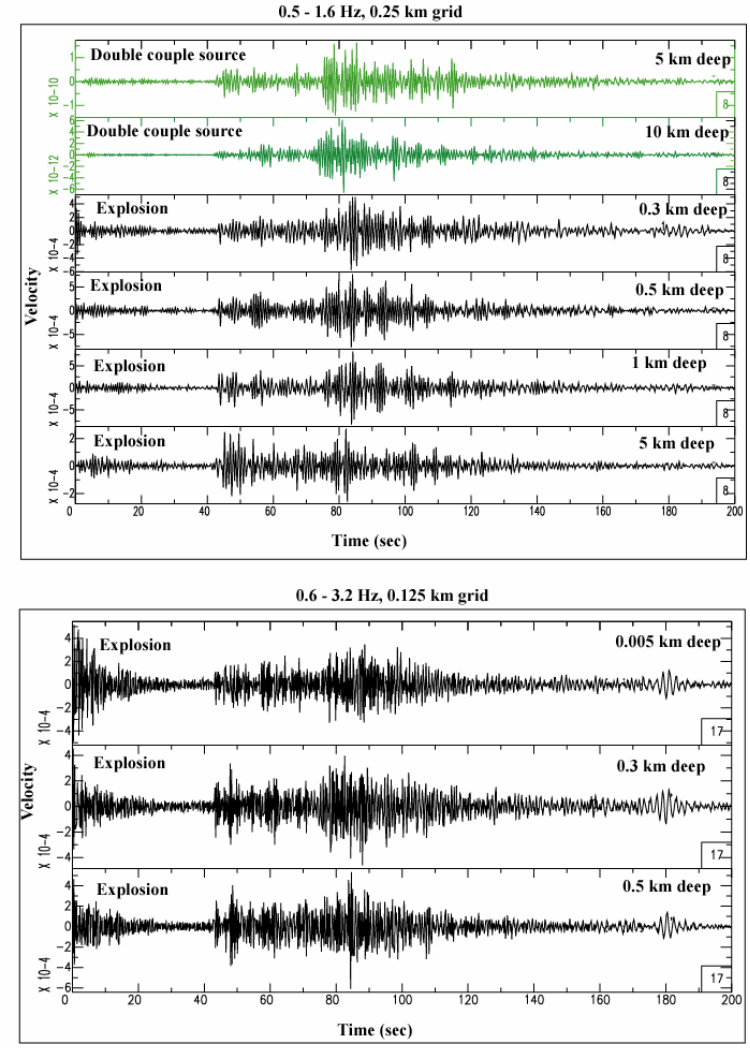

Figure 4. Synthetic seismograms for earthquakes and explosions at different depths for 0.25 km grid size (upper plots) and 0.125 km grid size (lower plots) in model SD5. The frequency range, mechanism, and depth are shown for each plot. Note less high-frequency energy with increasing depth. Also note a model artifact (due to the sharp variation in heterogeneity at 6 km depth) at time lag 180 sec.

CONCLUSIONS

Studies of seismic and borehole data at NTS have the potential to provide constraints for the stochastic model parameters. Reliable coda modeling is only possible when considering the entire waveform. While the effect of Moho depth and the source mechanism is important for direct *P* and Lg, their effect is less important for the *Lg* coda than the effect of the heterogeneity location relative to the model surface. Seismic velocity perturbations and correlation length are important for *Lg* coda shape, and their values can be constrained by fitting the first arrivals as well. So far, we have considered a simple 2D deterministic model for the path between the NTS and MNV. A 3D model consisting of laterally inhomogeneous structures will affect the coda energy partitioning. In a future model, the heterogeneity edge will need to be smoothed.

The next stage of modeling development will be the addition of attenuation and topography. We will use digital elevation models for NTS in order to simulate *Rg* scattering from topography, which has been shown to be a primary constituent of explosion-generated shear waves. This scattering will contribute to the coda signatures for our synthetics. We will then systematically modify the random velocity heterogeneities to improve the match between the observed and synthetic data. Three dimensional strip models will also be developed to examine the scattering

efficiency of 2D media in comparison to 3D simulations. Multiple runs with different realizations of stochastic velocity will be needed to find average amplitude envelopes of the seismic traces for every set of the stochastic parameters. These parameters will then be calibrated by matching synthetic earthquake *Sn* and *Lg* coda envelopes to local earthquakes with well-defined moments and mechanisms. We will quantify possible biases in the yields between test sites and relate them to the choice of, or combination of, *Sn* and *Lg* mechanisms. Finally, we will use our techniques to estimate the *Sn* and *Lg* coda spectra for explosions in uncalibrated regions.

ACKNOWLEDGEMENTS

We thank Mr. Allen Cogbill for providing velocity data at Pahute Mesa and professor John Fergusson for help with the Pahute Mesa well log data. We wish to thank Dr. Jeffrey Orrey for his continued support on the GFM2D/3D code.

REFERENCES

Benz, H. M., Unger, J. D., Leith, W. and V. Ryaboy (1991). The Norilsk DSS Profile in Northern Siberia: interpretation of the velocity structure and comparison with basin and range and New England profiling results, in *Abstracts of the 13th Annual PL/DARPA Seismic Research Symposium*, 85–100.

Dainty, A. M. and M.N. Toksoz (1990). Array analysis of seismic scattering, *Bull. Seism. Soc. Am.*, 80: (6), 2242–2260.

Der, Z., M. E. Marshall, A. O'Donnell, and T. W. McElfresh (1984). Spatial coherence structure and attenuation the *Lg* phase, site effects, and interpretation of the *Lg* coda, *Bull. Seism. Soc. Am.* 74: 1125–1148.

Ferguson, J.F., Cogbill, A.H., and Warren, R.G. (1994). A geophysical-geological transect of the Silent Canyon caldera complex, Pahute Mesa, Nevada, *J. Geophys. Res.* 99: 4323–4339.

Frankel, A. and R.W. Clayton (1986). Finite difference simulations of seismic scattering: implications for the propagation of short-period seismic waves in the crust and models of crustal heterogeneity. *J. Geophys. Res.* 91: No. B6: 6465:6489.

Mayeda, K. M. (1993). mb(*Lg*Coda): a stable single station estimator of magnitude, *BSSA,* 83: 851–861.

Mayeda K. and W. Walter (1996). Moment, energy, stress drop, and source spectra of western U.S. earthquakes. *J. Geophys. Res.* 101**:** 11195–11208.

McLaughlin, KL, L. R. Johnson, LR and T.V. McEvilly (1983). Two-dimensional array measurements of near-source ground accelerations, *Bull. Seis. Soc. Am.* 73:349–375.

Nishizawa, O., T. Satoh, X. Lei, and Y. Kuwahara (1997). Laboratory studies of seismic wave propagation in inhomogeneous media using a laser Doppler vibrometer, *Bull. Seism. Soc. Am.* 87**:** 809 –823.

Orrey, J. L., C. B. Archambeau and G. A. Frazier (2002). Complete seismic wavefield synthesis with a pseudospectral method: The Generalized Fourier Method, revised manuscript to be submitted to *Geophys. J. Int.*

Pullammanapalil, S., A. Levander, S. Larkin (1997). Estimation of crustal stochastic parameters from seismic exploration data, *J. Geophys. Res*. 102: 15269–15286.

Rautian, T. G. and V. I. Khalturin (1978). The use of the coda for determination of the earthquake source spectrum, *Bull. Seism. Soc. Am.* 68: 923–948.

Scherbaum F., D. Gillard and N. Deichmann (1991). Slowness power spectrum analysis of the coda composition of two microearthquake clusters in northern Switzerland, *Phys. Earth. Planet. Inter*. 67: 137–161.

Shapiro, N. M., M. Campillo, L. Margerin, S. K. Singh, V. Kostoglodov, and J. Pacheco (2000). The Energy Partitioning and the Diffusive Character of the Seismic Coda, *Bull. Seis. Soc. Am.* 90: (3), 655–665.

Springer, D. L., G. A. Pawloski, J. L. Ricca, R. F. Rohrer and D. K. Smith (2002). Seismic source summary for all U. S. below surface nuclear explosions, *Bull. Seism. Soc. Am.* 92: 1806–1846.

Spudich, P., and Bostwick, T. (1987). Studies of the seismic coda using an earthquake cluster as a buried seismograph array, *J. Geophys. Res.* 92: 10526–10546.

Stevens, J. L., T. G. Berker, S. M. Day, K. L. McLaughlin, N. Rimer and B. Shkoller (1991). Simulation of teleseismic body waves, regional seismograms, and Rayleigh wave phase shifts using two-dimensional, nonlinear models of explosion sources, *Explosion Source Phenomenology, Geophysical Monograph 65*, Copyright 1991, American Geophysical Union: 239–252.

Stump, B. W. and L. R. Johnson (1984). Near-field source characterization of contained nuclear explosions in tuff, *Bull. Seism. Soc. Am.* 74: 1–26.

Tibuleac, I. M., A. Stroujkova, J. L. Bonner and K. Mayeda (2005). Predicting explosion generated Lg and Sn using synthetic seismograms, in *27th Seismic Research Review: Ground-Based Nuclear Explosion Monitoring Technologies*, Vol. 1, pp. 214–221.

Xie, J., L. Cong, B.J. Mitchell, and J.-M. Chiu (1996). Complexities in high-frequency seismic waveforms due to three-dimensional structure in the New Madrid Seismic Zone, *J. Geophys. Res.* 101: (B3): 5751–5778.